



# A high yield, one-pot dialysis-based process for self-assembly of near infrared absorbing gold nanoparticles



Dhruvinkumar Patel, Kurtis T. James, Martin O'Toole\*, Guandong Zhang, Robert S. Keynton, André M. Gobin

Department of Bioengineering, University of Louisville, Louisville, KY 40292, United States

## ARTICLE INFO

### Article history:

Received 4 September 2014

Accepted 10 November 2014

Available online 18 November 2014

### Keywords:

Gold nanoparticles

Near infrared

Synthesis

Coating

Dialysis

DiaSynth

## ABSTRACT

**Hypothesis:** A facile, dialysis-based synthesis of stable near infrared (nIR) absorbing plasmonic gold nanoparticles ( $\lambda_{\text{max}} = 650\text{--}1000\text{ nm}$ ) will increase the yield of nIR particles and reduce the amount of gold colloid contaminant in the product mixture.

**Experiments:** Chloroauric acid and sodium thiosulfate were reacted using a dialysis membrane as a reaction vessel. Product yield and composition was determined and compared to traditional synthesis methods. The product particle distribution, yield, and partitioning of gold between dispersed product and membrane-adsorbed gold were determined.

**Findings:** The synthesis results in polydisperse particle suspensions comprised of 70% spheroid-like particles, 27% triangular plates, and 3% rod-like structures with a 3% batch-to-batch variation and a prominent nIR absorption band with  $\lambda_{\text{max}} = 650\text{--}1000\text{ nm}$ . The amount of small gold colloid ( $\lambda_{\text{max}} = 530\text{ nm}$ ;  $d < 10\text{ nm}$ ) in the isolated product was reduced by 96% compared to traditional methods. Additionally, 91.1% of the gold starting material is retained in the solution-based nanoparticle mixture while 8.2% is found on the dialysis membrane. The synthesis results in a quality ratio (QR =  $\text{Abs}^{\text{nIR}}/\text{Abs}^{530}$ ) of 1.7–2.4 (twice that of previous techniques) and 14.3 times greater OD\*ml yield of the nIR-absorbing nanoparticle fraction.

© 2014 Elsevier Inc. All rights reserved.

## 1. Introduction

The production of gold nanostructures such as nanoplates, nanoshells, and nanorods with plasmon resonance frequencies in the near infrared (nIR) region of the electromagnetic spectrum is currently an area of growing research focus [1–4]. The importance of the nIR region (650–900 nm) in medicine is due to the high transmission and low absorption of light by native tissue components, such as water and hemoglobin [6–8]. Thus, nIR light has minimal interference with tissue and interacts strongly with exogenous materials that absorb nIR light. This enables targeted drug

delivery and biosensing, as well as combined therapeutic and imaging (theranostics) capabilities such as nIR imaging and photothermal treatment *in situ* [7,9–14].

To date, a number of methods have been employed to synthesize gold nanoparticles (GNPs), including nanoshells [15–19], nanorods [20–27], nanocages [28–30], nanostars [31–34], and nanoplates [35–51] that absorb in the nIR spectral region. Although these methods produce nIR-GNPs, they are typically seed mediated syntheses that require multiple steps, use toxic agents, difficult to remove surfactants (i.e. CTAB) or require laborious purification steps that significantly reduce product yield. However, of the above mentioned techniques, one of the most promising approaches to synthesizing nIR particles is through the reaction of chloroauric acid (HAuCl<sub>4</sub>) with a sulfur-containing reducing agent (i.e. sodium sulfide or sodium thiosulfate) using either a 1- or 2-step process [49,50,52–58]. The reaction with either of the sulfur reagents can be performed at room temperature and produce similar products. Sodium sulfide (Na<sub>2</sub>S) is typically “aged” for several days in solution, prior to the reaction, during which time sodium thiosulfate (Na<sub>2</sub>S<sub>2</sub>O<sub>3</sub>) and potentially other oxidized sulfur species

**Abbreviations:** nIR, near infrared; GNP, gold nanoparticle; nIR-GNP, near infrared absorbing gold nanoparticle; CTAB, cetyltrimethylammonium bromide; QR, quality ratio; Abs, absorbance; MWCO, molecular weight cutoff; SEM, scanning electron microscopy; OD, optical density.

\* Corresponding author at: Department of Bioengineering, University of Louisville, Rm. 411 Lutz Hall, Louisville, KY 40292, United States. Fax: +1 502 852 6806.

E-mail addresses: [dnpatel01@gmail.com](mailto:dnpatel01@gmail.com) (D. Patel), [kurtis.james@louisville.edu](mailto:kurtis.james@louisville.edu) (K.T. James), [martin.otoole@louisville.edu](mailto:martin.otoole@louisville.edu) (M. O'Toole), [guandongzhang@hotmail.com](mailto:guandongzhang@hotmail.com) (G. Zhang), [rob.keynton@louisville.edu](mailto:rob.keynton@louisville.edu) (R.S. Keynton), [iamgobin@gmail.com](mailto:iamgobin@gmail.com) (A.M. Gobin).

( $S_2O_6^{2-}$ ,  $SO_4^{2-}$ , or  $SO_3^{2-}$ ) are generated [54]. The products of this reaction are separated into two major classes: colloidal gold nanoparticles (2–10 nm diameter) with a plasmon resonance peak at  $\sim 530$  nm, and a nIR-absorbing fraction (nIR-GNP) with a resonance wavelength that can vary from 650 to 2000 nm depending on the synthesis conditions. The particle sizes and geometries reported in the literature for the nIR-absorbing fraction vary widely and are typically polydisperse, with spheroids, triangular nanoplates, nanorods, and various other polyhedra ranging in size from 30 to 100 nm [52,55,56]. While the identity of the spheroidal particles in the nIR fraction is the subject of considerable debate (colloidal aggregates vs. gold/gold sulfide nanoshells), the present work is primarily concerned with increasing the yield of the triangular nanoplates, which show intense absorption in the nIR range [7,49,51–55,59–61]. In addition to the intense nIR absorbance of gold nanoplates, the plasmon resonance frequency is dependent on the geometric properties of the plates (i.e. edge length, plate thickness, and vertex shape) and is therefore tunable depending on the reaction conditions used for synthesis [42,50,62].

Unfortunately, uptake of some non-therapeutic (non-nIR) particles has the potential to lead to increased oxidative stress and immune response [63–65]. For therapeutic applications, the colloidal gold fraction can be considered a contaminant and is typically separated from the nIR-absorbing fraction through multiple rounds of centrifugation [7]. While effective, this purification process results in a significant loss in the yield of therapeutic particles that remain within the supernatant or experience irreversible aggregation.

The ratio of absorbances (optical densities, OD) of the nIR resonance maximum ( $Abs^{nIR}$ ) to the absorbance maximum for colloidal gold ( $Abs^{530nm}$ ), herein defined as the quality ratio ( $QR = Abs^{nIR}/Abs^{530nm}$ ), can be used to assess the purity of a particular batch of particles in terms of nIR content. Typical “traditional” synthesis processes have been shown to produce QRs ranging from 0.8 to 1.2 [7,13,50,52,54]. However, after multiple rounds of centrifugation, the QR has been shown to improve to between 1.5 and 2.0, respectively [7,50].

As a result, significant room for improvement exists in the production of nIR particles through the gold salt/sulfur reductant route in terms of maximizing the yield of the nIR fraction, eliminating colloidal contaminant in the final product, improving the tunability of the nIR resonance frequency, and improving the reproducibility of the morphologies of the nIR-GNP. Therefore, the purpose of this work is to report on a new one-pot synthesis methodology, called DiaSynth, which uses a regenerated cellulose dialysis membrane as a reaction vessel to react  $H AuCl_4$  with  $Na_2S_2O_3$  to reproducibly synthesize nIR-GNPs in high yield without additional purification processes. This self-assembly process also enables *in situ* coating of nanoparticles and auxiliary utilization of the dialysis membrane as an effective tool to separate the coated product from the excess coating molecules.

## 2. Results and discussion

### 2.1. Non-Dialysis synthesis route

For comparison of the proposed dialysis-based synthesis approach, we have chosen the previously reported 1-step reaction between chloroauric acid and sodium thiosulfate as a model for a typical synthesis of these particles in the literature [54]. Upon mixing of the gold and thiosulfate solutions, a burgundy/gray suspension quickly developed. Progress of the reaction was followed via UV–visible spectroscopy, which revealed that the spectrum of the mixture remains constant after 1 h, implying completion of the reaction, Fig. 1. A typical quality ratio ( $QR = Abs^{nIR}/Abs^{530nm}$ ) for

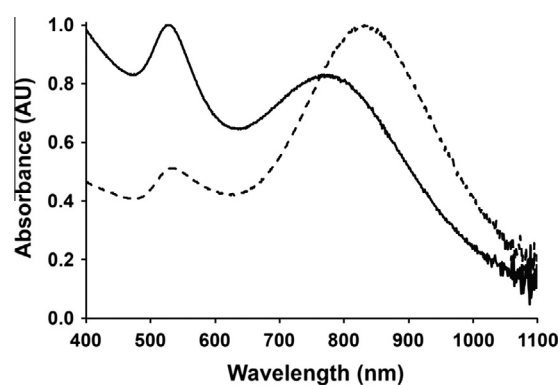


Fig. 1. Normalized spectral profiles of the products from the traditional 1-step method with chloroauric acid and sodium thiosulfate before (solid line) and after (dashed line) a  $3\times$  centrifugation process.

the reaction at this point is 0.83, implying that colloidal gold is abundant in the product mixture. The hydrodynamic diameter (via dynamic light scattering) and zeta potential measurements of these particles were 34.4 nm and  $-34.6$  mV, respectively. After combining the pellets from three rounds of centrifugation (1150g, 20 min) and re-suspending in DI  $H_2O$ , the UV–vis spectrum of the suspension reveals that the QR has increased to 1.95, indicating that nIR particles have been separated during purification. The hydrodynamic diameter and zeta potential of the sample remain relatively unaffected by the centrifugation process, measuring 34.8 nm and  $-36.9$  mV, respectively.

The selection of  $Na_2S_2O_3$  over  $Na_2S$  was made due to several factors. Optimal literature preparations using  $Na_2S$  require aging the  $Na_2S$  solution for several months [54]. The volume of  $Na_2S$ , its concentration, and duration of aging all potentially effect the position of the nIR peak of the product nIR-GNPs. This has been attributed to a chemical change during the aging process of  $Na_2S$  solution, where  $Na_2S_2O_3$  is the likely product due to oxygen exposure to form sulfur oxide species [54]. Additionally, compared to the  $Na_2S$  solution, the  $Na_2S_2O_3$  solution is more stable and its aging has no effect on the synthesis [54].

The  $Na_2S_2O_3$  plays two roles during the GNP synthesis: reducing agent for reduction of  $Au^{3+}$  to elemental Au, and capping agent. In the second role,  $Na_2S_2O_3$  consumed during the reaction produces a variety of sulfur-based compounds (e.g.  $S_2O_6^{2-}$ ,  $SO_4^{2-}$ , or  $SO_3^{2-}$ ), that are potential capping agents that can bind to the gold particle and contribute to asymmetric gold crystal growth [54]. Despite the variety of nanostructure morphologies in the product mixture, all

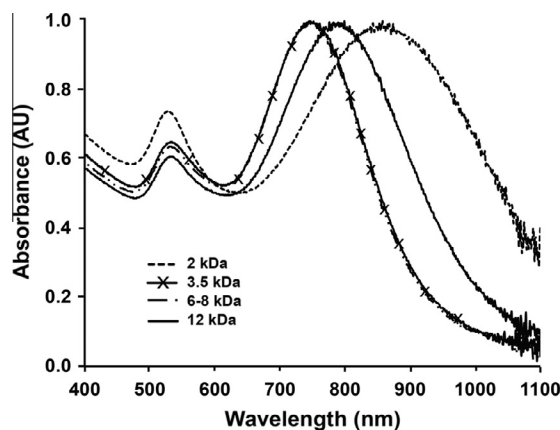


Fig. 2. Normalized spectral profiles of the products from DiaSynth with 2, 3.5, 6–8, and 12 kDa MWCO dialysis membranes.

**Table 1**

Hydrodynamic diameter, zeta potential, quality ratio (QR) and absorbance maxima for products from the traditional 1-step synthesis and DiaSynth with various MWCO dialysis membranes.

MWCO (kDa)	Hydrodynamic diameter (nm)	Zeta potential (mV)	QR ( $Abs_{nIR}/Abs_{530nm}$ )	$\lambda_{max}$ (nm)
0	34.4	−34.6	0.83	773
2	48.75	−26.4	1.35	859
3.5	58.77	−35.3	1.54	744
6–8	62.90	−29.9	1.57	747
12	60.23	−30.3	1.65	799

of the structures produced by the reaction, seem to be typified by a fcc lattice structure [51].

## 2.2. Synthesis of nIR gold nanoparticles in regenerated cellulose membrane (DiaSynth)

The DiaSynth process is analogous to the traditional 1-step synthesis with the exception of utilizing a dialysis membrane as a reaction vessel submerged in DI water. Molecular weight cut-offs (MWCO) of 2, 3.5, 6–8, and 12 kDa were utilized. The reaction is complete after a 1 h period. The normalized spectral profiles for the reaction product for DiaSynth, as well as the traditional 1-step synthesis are displayed in Fig. 2. The average hydrodynamic diameter, zeta potential,  $\lambda_{max}$ , and QR for each batch can be found in Table 1.

The average particle size derived from the DiaSynth procedure for all MWCO dialysis membranes is larger than those from the non-dialysis method. Similarly, a shift in particle population toward nIR-GNPs, where the particle morphology is dominated by 30–40 nm multi-faceted spheroid-like particles and 60–80 nm triangular nanoplates, *vide infra* [51]. These lower-symmetry structures have been shown to absorb strongly in the nIR region, compared to spherical particles that absorb primarily between 520 and 580 nm. As the MWCO of the dialysis membrane is increased, both the average hydrodynamic diameter and QR of the particles also increase. There was also an initial blue shift in the nIR absorbance

maximum as the MWCO increased up until 6–8 kDa, with the 3.5 kDa and 6–8 kDa membranes producing nIR peaks near 750 nm. However, when the MWCO is increased to 12 kDa, a red shift occurs that places the nIR maximum at 799 nm. The highest QR ratio (QR = 1.65) was produced by the 12 kDa membrane. The zeta potential for each batch varies between −26.4 mV and −35.3 mV for the various MWCO with no discernible trend between MWCO and zeta potential. All particle suspensions, regardless of MWCO, were found to remain stable for several weeks based on the nIR absorbance values (data not shown).

## 2.3. Comparison of DiaSynth to traditional 1-step synthesis

TEM imaging of the particles from both the non-dialysis and DiaSynth (12 kDa MWCO) routes reveal very similar sizes and morphologies for the larger spheroid, rod, and triangular shaped particles, Fig. 3. For both samples, spheroidal particles with diameters ranging from 20 to 40 nm and triangular plates with edge lengths of 50–100 nm are prevalent.

There is, however, based on ImageJ [66] software analysis of the images, a 96% decrease in colloidal gold (<10 nm) present in the DiaSynth samples compared to the non-dialysis samples.

This coincides with the shift to higher hydrodynamic diameters and QR for the DiaSynth samples as colloidal gold is not as prevalent in the product mixture. Statistical analysis of the DiaSynth TEM images reveals a nIR-absorbing particle distribution of 70% spheroid-like (diameter  $\sim$ 33.5 nm), 27% triangular plates (apex  $\sim$ 80 nm), and less than 3% others (rods, truncated octahedrons, length  $\sim$ 75.1 nm), Table 2. By comparison, the traditional 1-step procedure leads to a nIR-absorbing particle distribution of 79% spheroid-like (diameter  $\sim$ 21.8 nm), 18% triangular plates (apex  $\sim$ 35.6 nm), and 3% others (length  $\sim$ 73.0 nm). Although both methods produce a very similar nIR-absorbing particle distribution, the near elimination of colloidal gold in the DiaSynth product presents a far superior approach to producing batches of nIR-absorbing particles. It is important to note, the nIR peak is dependent on the size of the triangular plates (i.e. apex  $\sim$ 40 nm and  $\sim$ 65 nm show nIR peak of 700 and 800 nm, respectively); therefore, synthesis parameters (i.e. concentration, volume, MWCO membrane, etc.) can be

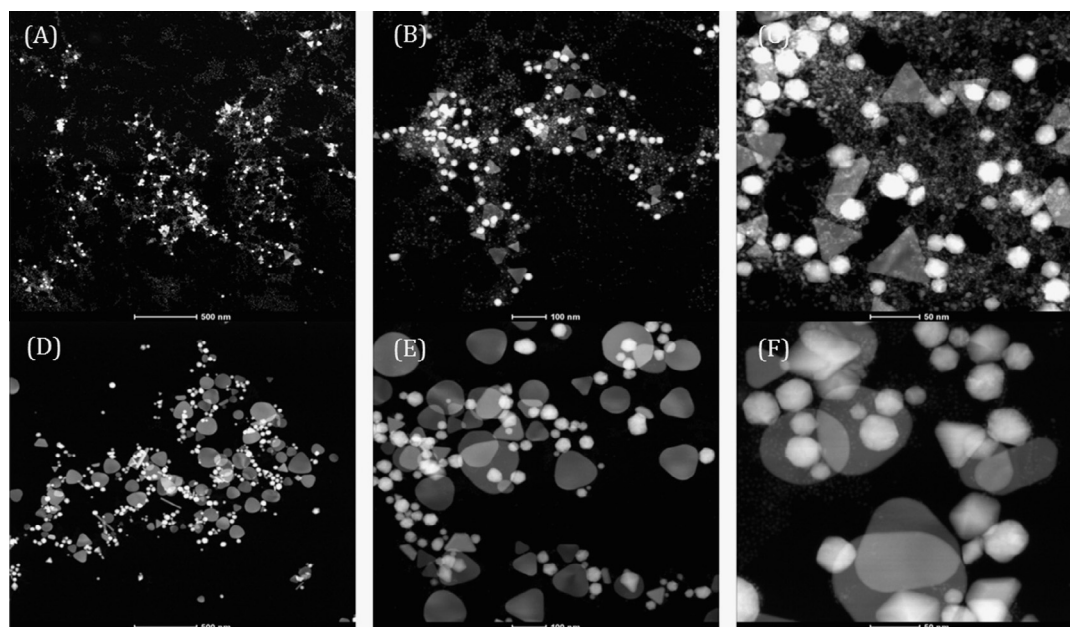


**Fig. 3.** TEM images of particles from the traditional 1-step synthesis (A–C) at different magnifications, and the DiaSynth Process (D–F) at different magnifications demonstrating the greatly reduced colloidal gold contamination found in the DiaSynth process.

**Table 2**  
GNPs size and percent analysis of DiaSynth and Traditional one-step synthesis.

	Traditional one-step		DiaSynth	
	Size (nm)	Percent	Size (nm)	Percent
Spheres	21.8	78.7	33.5	70
Plates	35.6	18	80.0	26.7
Other	73	3.3	75.1	3.3

**Table 3**  
Yield calculations for DiaSynth and the traditional 1-step synthesis methods.

	DiaSynth	Non-dialysis
As made	55 mLs @ 7.5 OD	55 mLs @ 2.5 OD
After multistep centrifugation	–	0.34 mLs @ 117 OD
Final yield (OD · mL)	412.5	28.9
Quality ratio	2.36	2.38

OD = optical density.

modified to adjust the size of triangle plate formation to favor a specific nIR peak. There is only a 3% variation in product morphology distribution between batches for the DiaSynth process, suggesting that despite the polydisperse nature of the product particles the DiaSynth process leads to a highly reproducible product distribution. This reproducibility in particle morphology may be due to the high volume of dialysate (8 L) acting as a temperature buffer that provides a relatively consistent environment around the surface of the dialysis membrane during the reaction process.

To directly compare the overall yield of the DiaSynth process with the traditional 1-step synthesis, batches of nanoparticles were fabricated using each method with identical reaction volumes, Table 3. The optical densities (OD) of both samples were measured after the initial reaction. Due to the presence of colloidal gold in the traditional 1-step synthesis, multiple centrifugation steps are required to purify the nIR fraction, whereas the DiaSynth process requires no centrifugation step. The significance of the loss of product during the centrifugation process can be determined by calculating the yield of each reaction as OD · mL. Although the quality ratios of the DiaSynth and post-centrifugation traditional process samples are nearly identical, 2.36 and 2.38, respectively, the yield of the nIR-absorbing fraction for DiaSynth is 14.3 times higher than the traditional synthesis. It is important to note that, for the centrifugation steps, utmost care was taken to maximize yield and that the highest possible centrifugation speed that did not result in irreversible sample aggregation was used.

#### 2.4. Analysis of the membrane

The dialysis membrane used in the DiaSynth reaction acquires an intense red/purple color following synthesis, implying that gold particle formation is happening on or within the membrane itself, or that particles forming in solution are adsorbing to the membrane. In order to elucidate the mechanism by which the regenerated cellulose membrane is facilitating an increase in nIR particle yield, the dialysis membrane used in the 12 kDa MWCO synthesis was analyzed by UV–visible spectroscopy and SEM imaging. The UV–visible spectrum of the dialysis membrane has peaks near the same location as the product mixture at both 532 nm and 840 nm; however, the relative intensities of the peaks are reversed compared to the liquid mixture, Figs. 2 and 4(A). This implies that the membrane appears to predominantly either sequester or seed the colloidal gold product. There is precedent in the literature for regenerated cellulose membranes acting both as reductants and scaffolds for the production of colloidal gold nanoparticles [67–70].

The carbonyl groups of the acetyl esters have been postulated to form coordinate bonds to gold atoms that later serve as nucleation sites for particle growth, while hydroxyl groups can directly reduce the gold ions to facilitate particle formation [67]. Indeed, the introduction of chloroauric acid into a 12 kDa MWCO regenerated cellulose membrane without any sulfur reducing agent leads to the formation of colloidal gold particles with an intense absorbance maximum at 530 nm and no detectable peak in the nIR region (data not shown). At room temperature, this reaction occurs at a slower time scale (observable color change within 1 h) than the reaction with thiosulfate (nearly instantaneous color change). It is therefore doubtful that the membrane itself is contributing to production of nIR-absorbing particles.

The UV–visible spectrum of the regenerated cellulose membranes after reaction with chloroauric acid in the absence of other reducing agents contains an intense absorbance at 530 nm, Fig. 4(B). The lack of significant nIR absorbance again precludes the participation of the membrane in production of nIR-GNP. The presence of a nIR absorbance in the membrane after the DiaSynth process is performed, suggests that nIR particles are simply adsorbing to the membrane, while colloidal particles are potentially both being seeded on as well as adsorbing to the membrane. SEM imaging of the 12 kDa regenerated cellulose membrane after DiaSynth reveals the presence of a large number of nearly spherical particles with diameters of less than 10 nm, Fig. 5. It is assumed that the absorbance in the nIR region of the membrane is due to these aggregated clusters of large spheroid gold particles and nanoplates. Examination of the SEM images of the DiaSynth membrane reveals a small (<1%) amount of triangular plates adsorbed to the membrane, which are the likely source for the nIR absorbance of the membrane.

#### 2.5. Analysis of the dialysate

In order to determine if gold particles were forming outside of the dialysis membrane, the dialysate from the DiaSynth process using a 12 kDa MWCO membrane was concentrated using a Rotovap down to ~20 mL. At this concentration, the dialysate acquired a faint red color and displayed an absorbance at 530 nm. It was initially unclear whether the particles are forming inside of the membrane and then dialyzing out, or that the starting materials are dialyzing out through the membrane and then forming nanoparticles outside of the membrane. Given the average number of gold atoms in 2 and 3 nm gold nanoparticles has been determined to be 144 and 479, respectively [5,71], the associated molecular mass for these particles (based solely on the gold core) would be

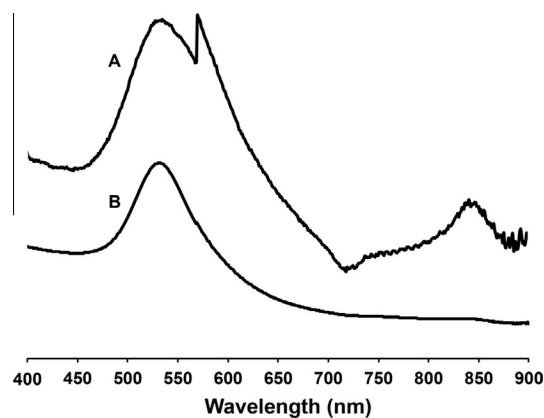


**Fig. 4.** UV–visible spectra of the dialysis membranes after (A) DiaSynth and (B) after reacting chloroauric acid (no external reducing agent) in a 12 kDa dialysis membrane.

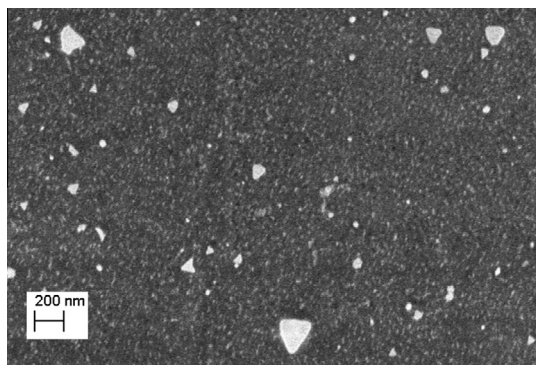


Fig. 5. SEM image of particles adsorbed to a 12 kDa dialysis membrane after the DiaSynth process.

28.4 kDa and 94.3 kDa, respectively. Thus, this implies that even 2 nm particles are too large to traverse the largest MWCO dialysis membranes used in this study (12 kDa), which suggests that the particles found in the dialysate are most likely forming outside of the dialysis membrane as gold precursors are dialyzed out of the reaction mixture. Indeed, measuring the conductance of the dialysate during a DiaSynth reaction shows a concomitant increase in conductivity compared to control samples during the timeframe of reaction, Fig. 6. This data suggests that particles are forming outside of the dialysis membrane as salts exit through the membrane during the reaction.

#### 2.6. Partitioning of gold between solution and membrane

In order to determine the percentage of gold starting material that remains trapped in the regenerated cellulose membrane, sodium cyanide was added to both 13.5 ml of the product mixture in a 25 ml beaker and an equal volume of water containing the regenerated cellulose membrane placed in a separate 25 ml beaker to sequester all of the gold from the nanoparticles to form cyanoaurate complexes [72,73]. After treatment with cyanide, the absorbance of the samples at 215 nm is directly related to the amount of cyanoaurate complexes formed, and thus, the amount of gold in each portion of the product. For DiaSynth with the 12 kDa MWCO membranes, 91.1% of the gold starting material is present in the solution-based nanoparticle mixture and 8.2% is found on the dialysis membrane. The remaining amount presumably is dialyzed out during the reaction, leading to the appearance of colloidal gold in the concentrated dialysate, *vide supra*. With knowledge of the per-

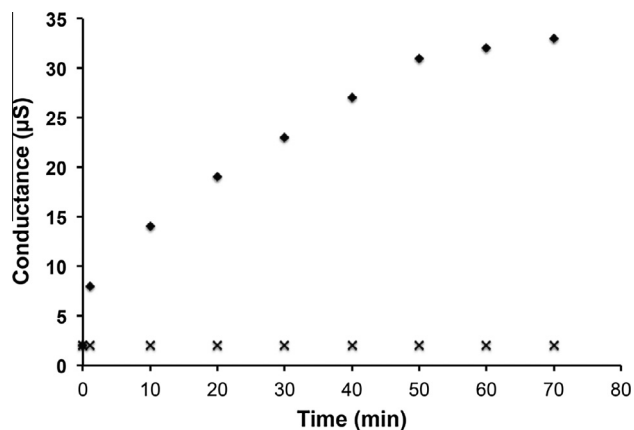


Fig. 6. Conductivity measurements of the dialysate during a DiaSynth reaction (◆) and during the same time period with just water in the dialysis membrane (X).

centages of colloid adsorbed on the membrane and the increased numbers and sizes of the nIR particles in the DiaSynth method, it becomes possible to suggest a possible mechanism regarding the progress of particle growth during DiaSynth. The DiaSynth process, due to the fast mixing of reagents and quick product formation, can be considered as a burst nucleation of small particle seeds from a supersaturated solution of reagents followed by a period of diffusional growth of particles [74]. During such processes, seed nucleation continues until the local concentration of monomers is depleted, and nucleation slows. At the same time, some of the colloidal gold seeds are adsorbed onto the dialysis membrane, thereby removing them from the reaction mixture, and leaving the remaining monomers to participation in diffusional growth of the particles remaining in suspension. The removal of seed particles by the membrane facilitates the growth of the remaining particles into larger sizes than in the traditional synthesis method.

#### 2.7. Surface coating reactions

The use of gold nanoparticles typically requires the addition of a surface coating to tailor the chemical functionality at the nanoparticle surface to a particular application [15–17,75]. The presence of the dialysis membrane as a reaction vessel in Diasynth provides a convenient “one-pot” system for both the synthesis of particles and coating within the same apparatus. After 1 h following initiation of a 12 kDa DiaSynth reaction, an excess of PEG-thiol (MW 5000 Da) was added to the dialysis membrane, and the mixture was allowed to dialyze overnight. The following day the mixture was transferred to a round-bottom flask and the water evaporated under reduced pressure on a Rotovap to a concentration of 651 OD with no loss in particle stability. This particle concentration value was chosen since it would lead to instant aggregation and precipitation in non-coated samples. The hydrodynamic diameters of the particles were found to increase from 41.55 to 48.46 nm after the coating reaction, confirming the presence of the PEG coating. This one-pot synthesis and coating technique eliminates the need to first isolate the newly synthesized particles from any reaction byproducts and allowing direct coating and purification of the coated particles *in situ*.

#### 2.8. Conclusions

The DiaSynth method for synthesis of nIR-absorbing gold nanoparticles represents a promising method for maximizing the yield of nIR-GNPs whilst dramatically reducing the amount of gold colloid contaminant (<10 nm) in the final product mixture. Indeed, the Diasynth method produces a distribution of nIR-absorbing particle morphologies nearly identical to traditional approaches, but with 14.3 times higher OD\*ml yield along with a 96% reduction in colloidal contamination. This method eliminates product loss from the time-consuming centrifugation steps required for similar levels of purity indicated in the literature. The product is suitable for use in nIR applications without any further purification (QR > 2.0). The nanoparticles can also be coated effectively *in situ* with thiol-containing molecules using the dialysis membrane as an effective tool to separate the coated product from excess coating molecules.

### 3. Experimental

#### 3.1. Chemical supplies

Hydrogen tetrachloroaurate (III) trihydrate (chloroauric acid,  $\text{HAuCl}_4 \cdot 3\text{H}_2\text{O}$ ) was purchased from Alfa Aesar (36,400). Sodium Thiosulfate ( $\text{Na}_2\text{S}_2\text{O}_3$ ), sodium cyanide, and potassium dicyanoaurate(I)

were purchased from Sigma (380,016). mPEG-SH was purchased from LaysanBio. All materials were used as received unless otherwise noted.

### 3.2. Traditional 1-step synthesis of nIR-GNP

2.5 mL  $\text{Na}_2\text{S}_2\text{O}_3$  solution (3 mM) in ultra-pure DI  $\text{H}_2\text{O}$  was added rapidly to a 11 mL  $\text{HAuCl}_4 \cdot 3\text{H}_2\text{O}$  solution (1.71 mM) at room temperature for 1 h with no stirring. The visible/NIR absorption spectrum was measured after one hour at room temperature on a Carey 50 UV/Vis spectrophotometer (Varian, Agilent Technologies). A Malvern Zetasizer (ZS90) was used to characterize the nIR-GNP nanoparticles surface charge and average size. Further purification of the nIR fraction was achieved via three rounds of centrifugation (1150g, 20 min). The pellets from each centrifugation step are then combined for analysis analogous to the crude product. A FEI Tecnai F20 transmission electron microscope (TEM, FEI Co.) operated at 200 kV was used to determine nIR-GNP nanoparticle morphology. The TEM samples were prepared by dropping 80  $\mu\text{L}$  of nIR-GNP suspension onto C-flat Holey carbon film enhanced TEM grids followed by room temperature drying overnight.

### 3.3. DiaSynth synthesis of nIR-GNP

nIR-GNP nanoparticles were synthesized by mixing 11 mL of 1.71 mM  $\text{HAuCl}_4 \cdot 3\text{H}_2\text{O}$  and 2.5 mL of 3 mM  $\text{Na}_2\text{S}_2\text{O}_3$ , in regenerated cellulose dialysis membrane with molecular weight cut-offs (MWCO) of 2, 3.5, and 6–8 kDa (Spectrum Laboratories, Rancho Dominguez, CA) and 12 kDa (Sigma Aldrich, St. Louis, MO). The reaction mixture is dialyzed against 8 L of DI water with stirring for 1 h. The Spectral profile, hydrodynamic diameter, and zeta potential were obtained immediately following the synthesis. TEM samples were prepared and imaged in a fashion analogous to the products from the traditional synthesis route.

### 3.4. Membrane-bound gold nanoparticle synthesis

32.6 mL of 1.71 mM  $\text{HAuCl}_4 \cdot 3\text{H}_2\text{O}$  were placed in a 12 kDa MWCO regenerated cellulose membrane (43 mm  $\times$  17 cm) with 7.4 mL ultrapure water. The reaction was allowed to proceed undisturbed for 5 days, after which UV–visible spectra were obtained of the product and the cellulose membrane. Membranes spectra were acquired on a Cary 100 UV–vis spectrophotometer with film holder attachment.

### 3.5. mPEG-SH coating of DiaSynth product

nIR-GNP were synthesized by the DiaSynth process as mentioned above. Briefly, 1.71 mM  $\text{HAuCl}_4 \cdot 3\text{H}_2\text{O}$  and 3 mM  $\text{Na}_2\text{S}_2\text{O}_3$  were mixed in a 12 kDa dialysis membrane dialyzed against 8 L of DI water with stirring for 1 h. After 1 h, mPEG-SH (5000 Da) was added to the membrane with the nIR-GNP nanoparticles and the sample was reacted overnight. This allowed the sample to be coated with mPEG-SH, while simultaneously removing excess mPEG-SH.

### 3.6. Determination of weight fractions of gold from DiaSynth reaction

A DiaSynth reaction was performed as described above using 32.6 mL of 1.71 mM  $\text{HAuCl}_4$  and 7.4 mL of 3 mM  $\text{Na}_2\text{S}_2\text{O}_3$  in a 12 kDa MWCO regenerated cellulose membrane (43 mm  $\times$  17 cm). The reaction mixture was poured from the dialysis membrane into a beaker and the dialysis membrane was placed in an equal volume of water in a separate beaker. Both mixtures were titrated with 100 mM KOH until pH 10.5 was achieved. An excess of NaCN was

then added to both mixtures to disband the gold nanoparticles and the reactions were mixed on a rocking mixer for 1 h. A portion of each mixture was then loaded into a UV–vis cuvette and the absorbance value at 215 nm was recorded. The absorbance values were compared to a calibration curve made from the absorbance values of various concentrations of Potassium dicyanoaurate(I).

### 3.7. Determination of dialysate conductance during a DiaSynth reaction

8 mL of 3 mM  $\text{Na}_2\text{S}_2\text{O}_3$  was added to 44 mL of 1.71 mM  $\text{HAuCl}_4$  inside a 152 mm long 12 kDa cellulose membrane (76 mm Flat Width) and placed in 8 L of 25 °C DI water inside a square plastic tub with constant stirring. 1.8 mL of dialysate was collected between half the distance from the cellulose membrane to container wall at 0, 1, 10, 20, 30, 40, 50, and 60 min time intervals and the conductance measured using a NanoBrook ZetaPALS (Brookhaven Instruments, Holtsville, NY). This same experiment was performed with 52 mL of DI water within the membrane as a control.

### Author contributions

The manuscript was written through contributions of all authors. All authors have given approval to the final version of the manuscript.

### Funding sources

This work was funded by the grant from Wallace Coulter Foundation: Early Career Phase I award, and NSF-EPSCoR No. 0814194.

### Acknowledgment

The authors wish to acknowledge Jacek Jasinski for his assistance in obtaining TEM images of the particles.

### References

- [1] W. Cai, T. Gao, H. Hong, J. Sun, *Sci. Appl.* 1 (2008) 17.
- [2] P.K. Jain, K.S. Lee, I.H. El-Sayed, M.A. El-Sayed, *J. Phys. Chem. B* 110 (2006) 7238.
- [3] K. Cheng, Z. Cheng, *Curr. Med. Chem.* 19 (2012) 4767.
- [4] J.K. Young, E.R. Figueroa, R.A. Drezek, *Ann. Biomed. Eng.* 40 (2012) 438.
- [5] C.J. Ackerson, P.D. Jadzinsky, J.Z. Sexton, D.A. Bushnell, R.D. Kornberg, *Bioconjugate Chem.* 21 (2010) 214.
- [6] A.M. Gobin, M.H. Lee, N.J. Halas, W.D. James, R.A. Drezek, J.L. West, *Nano Lett.* 2007 (1929) 7.
- [7] A.M. Gobin, E.M. Watkins, E. Quevedo, V.L. Colvin, J.L. West, *Small* 6 (2010) 745.
- [8] R. Weissleder, *Nat. Biotechnol.* 19 (2001) 316.
- [9] X. Huang, P.K. Jain, I.H. El-Sayed, M.A. El-Sayed, *Nanomedicine (London England)* 2 (2007) 681.
- [10] A.R. Lowery, A.M. Gobin, E.S. Day, N.J. Halas, J.L. West, *Int. J. Nanomed.* 1 (2006) 149.
- [11] X. Sun, G. Zhang, D. Patel, D. Stephens, A.M. Gobin, *Ann. Biomed. Eng.* (2012).
- [12] Z. Xiao, C. Ji, J. Shi, E.M. Pridgen, J. Frieder, J. Wu, O.C. Farokhzad, *Angew. Chem. Int. Ed. Engl.* 51 (2012) 11853.
- [13] X. Sun, G. Zhang, R.S. Keynton, M.G. O'Toole, D. Patel, A.M. Gobin, *Nanomedicine* (2013).
- [14] Y. Li, A.M. Gobin, G.W. Dryden, X. Kang, D. Xiao, S.P. Li, G. Zhang, R.C. Martin, *Int. J. Nanomed.* 8 (2013) 2153.
- [15] M.C. Daniel, D. Astruc, *Chem. Rev.* 104 (2004) 293.
- [16] R. Mout, D.F. Moyano, S. Rana, V.M. Rotello, *Chem. Soc. Rev.* 41 (2012) 2539.
- [17] S. Rana, A. Bajaj, R. Mout, V.M. Rotello, *Adv. Drug Del. Rev.* 64 (2012) 200.
- [18] S.J. Oldenburg, J.B. Jackson, S.L. Westcott, N.J. Halas, *Appl. Phys. Lett.* 75 (1999) 2897.
- [19] S.J. Oldenburg, R.D. Averitt, S.L. Westcott, N.J. Halas, *Chem. Phys. Lett.* 288 (1998) 243.
- [20] B. Panchapakesan, B. Book-Newell, P. Sethu, M. Rao, J. Irudayaraj, *Nanomedicine (Lond.)* 6 (2011) 1787.
- [21] J. Perezjuste, I. Pastorizasantos, L. Lizmarzan, P. Mulvaney, *Coord. Chem. Rev.* 2005 (1870) 249.
- [22] C.J. Murphy, T.K. Sau, A.M. Gole, C.J. Orendorff, J. Gao, L. Gou, S.E. Hunyadi, T. Li, *J. Phys. Chem. B* 109 (2005) 13857.

- [23] S. Link, M.A. El-Sayed, *J. Phys. Chem. B*, 103 (1999) 8410.
- [24] B. Nikoobakht, M.A. El-Sayed, *Chem. Mater.* 2003 (1957) 15.
- [25] C.A.J. Foss, C.L. Hornyak, J.A. Stocked, C.R. Martin, *J. Phys. Chem.* 96 (1992) 7497.
- [26] C.R. Martin, *Science* 2006 (1961) 266.
- [27] C.R. Martin, *Chem. Mater.* 8 (1996) 1739.
- [28] S.E. Skrabalak, J. Chen, Y. Sun, X. Lu, L. Au, C.M. Copley, Y. Xia, *Acc. Chem. Res.* 41 (2008) 1587.
- [29] S.E. Skrabalak, L. Au, X. Li, Y. Xia, *Nat. Protoc.* 2 (2007) 2182.
- [30] Y. Xia, W. Li, C.M. Copley, J. Chen, X. Xia, Q. Zhang, M. Yang, E. Cho, P.K. Brown, *Acc. Chem. Res.* 44 (2011) 914.
- [31] C.L. Nehl, H. Liao, J.H. Hafner, *Nano Lett.* 6 (2006) 683.
- [32] P. Senthil Kumar, I. Pastoriza-Santos, B. Rodriguez-Gonzalez, F. Javier Garcia de Abajo, L.M. Liz-Marzan, *Nanotechnology* 19 (2008) 015606.
- [33] C.G. Khoury, T.J. Vo-Dinh, *Phys. Chem. C Nanomater. Interfaces* 112 (2008) 18849.
- [34] S. Trigari, A. Rindi, G. Margheri, S. Sottini, G. Dellepiane, E. Giorgetti, *J. Mater. Chem.* 21 (2011) 6531.
- [35] J.E. Millstone, S. Park, K.L. Shuford, L. Qin, G.C. Schatz, C.A. Mirkin, *J. Am. Chem. Soc.* 127 (2005) 5312.
- [36] S.S. Shankar, A. Rai, B. Ankamwar, A. Singh, A. Ahmad, M. Sastry, *Nat. Mater.* 3 (2004) 482.
- [37] F. Kim, S. Connor, H. Song, T. Kuykendall, P. Yang, *Angew. Chem. Int. Ed. Engl.* 43 (2004) 3673.
- [38] S. Kundu, L. Peng, H. Liang, *Inorg. Chem.* 47, 6344.
- [39] Z. Guo, X. Fan, L. Liu, Z. Bian, C. Gu, Y. Zhang, N. Gu, D. Yang, J. Zhang, *J. Colloid Interface Sci.* 348 (2010) 29.
- [40] J.E. Millstone, G.S. Métraux, C.A. Mirkin, *Adv. Funct. Mater.* 16 (2006) 1209.
- [41] R. Morarescu, H. Shen, R.A.L. Vallée, B. Maes, B. Kolaric, P. Damman, *J. Mater. Chem.* 22 (2012) 11537.
- [42] J.E. Millstone, S.J. Hurst, G.S. Métraux, J.I. Cutler, C.A. Mirkin, *Small* 5 (2009) 646.
- [43] C. Bao, N. Beziere, P. del Pino, B. Pelaz, G. Estrada, F. Tian, V. Ntziachristos, J.M. de la Fuente, D. Cui, *Small* 9 (2013) 68.
- [44] A. Miranda, E. Malheiro, E. Skiba, P. Quaresma, P.A. Carvalho, P. Eaton, B. de Castro, J.A. Shelnut, E. Pereira, *Nanoscale* 2 (2010) 2209.
- [45] T.H. Ha, H.-J. Koo, B.H. Chung, *J. Phys. Chem. C* 111 (2007) 1123.
- [46] G.P. Luke, A. Bashyam, K.A. Homan, S. Makhija, Y.S. Chen, S.Y. Emelianov, *Nanotechnology* 24 (2013) 455101.
- [47] J. Sun, M. Guan, T. Shang, C. Gao, Z. Xu, *Sci. China Chem.* 53 (2010) 2033.
- [48] K.L. Young, M.R. Jones, J. Zhang, R.J. Macfarlane, R. Esquivel-Sirvent, R.J. Nap, J. Wu, G.C. Schatz, B. Lee, C.A. Mirkin, *PNAS* 109 (2012) 2240.
- [49] B. Pelaz, V. Grazu, A. Ibarra, C. Magen, P. del Pino, J.M. de la Fuente, *Langmuir* 28 (2012) 8965.
- [50] G. Zhang, J.B. Jasinski, J.L. Howell, D. Patel, D.P. Stephens, A.M. Gobin, *Nanoscale Res. Lett.* 7 (2012) 337.
- [51] G.D. Zhang, X.H. Sun, J. Jasinski, D. Patel, A.M. Gobin, *J. Nanomater.* (2012).
- [52] R.D. Averitt, D. Sarkar, N.J. Halas, *Phys. Rev. Lett.* 78 (1997) 4217.
- [53] G. Raschke, S. Brogl, A.S. Susha, A.L. Rogach, T.A. Klar, J. Feldmann, B. Fieries, N. Petkov, T. Bein, A. Nichtl, K. Kurzinger, *Nano Lett.* 5 (2005) 811.
- [54] A.M. Schwartzberg, C.D. Grant, T. van Buuren, J.Z. Zhang, *J. Phys. Chem. C* 111 (2007) 8892.
- [55] H.S. Zhou, I. Honma, H. Komiyama, J.W. Haus, *Phys. Rev. B* 50 (1994) 12052.
- [56] J.J. Diao, H. Chen, *J. Chem. Phys.* (2006) 124.
- [57] T. Morris, H. Copeland, G. Szulcowski, *Langmuir* 18 (2002) 535.
- [58] T.J. Norman, J. Christian, D. Grant, D. Magana, J.Z. Zhang, J. Liu, D. Cao, F. Bridges, A. Van Buuren, *J. Phys. Chem. B* 106 (2002) 7005.
- [59] J.Z. Zhang, A.M. Schwartzberg, T. Norman, C.D. Grant, J. Liu, F. Bridges, T. van Buuren, *Nano Lett.* 5 (2005) 809.
- [60] X.H. Huang, P.K. Jain, I.H. El-Sayed, M.A. El-Sayed, *Nanomedicine* 2 (2007) 681.
- [61] Y.J. Huang, A.R. Ferhan, Y. Gao, A. Dandapat, D.H. Kim, *Nanoscale* 6 (2014) 6496.
- [62] K.L. Kelly, E. Coronado, L.L. Zhao, G.C. Schatz, *J. Phys. Chem. B* 107 (2003) 668.
- [63] Y. Pan, A. Leifert, D. Ruau, S. Neuss, J. Bornemann, G. Schmid, W. Brandau, U. Simon, W. Jahnhen-Dechent, *Small* 5 (2009) 2067.
- [64] M. Turner, V.B. Golovko, O.P.H. Vaughan, P. Abdulkina, A. Berenguer-Murcia, M.S. Tikhov, B.F.G. Johnson, R.M. Lambert, *Nature* 454 (2008) 981.
- [65] A.M. Alkilany, C.J. Murphy, *J. Nanopart. Res.* 12 (2010) 2313.
- [66] W.S. Rasband, National Institute of Health, Bethesda, MD, 1997–2011.
- [67] O.Y. Uryupina, V.V. Vysotskii, V.V. Matveev, A.V. Gusel'nikova, V.I. Roldughin, *Colloid J.* 73 (2011) 551.
- [68] S. Padalkar, J.R. Capadona, S.J. Rowan, C. Weder, Y.H. Won, L.A. Stanciu, R.J. Moon, *Langmuir* 26 (2010) 8497.
- [69] T.J. Zhang, W. Wang, D.Y. Zhang, X.X. Zhang, Y.R. Ma, Y.L. Zhou, L.M. Qi, *Adv. Funct. Mater.* 20 (2010) 1152.
- [70] K.A. Mahmoud, K.B. Male, S. Hrapovic, J.H.T. Luong, *Acs Appl. Mater. Interfaces* 1 (2009) 1383.
- [71] Y. Lu, L. Wang, D. Chen, G. Wang, *Langmuir* 28 (2012) 9282.
- [72] A.C. Templeton, M.J. Hostetler, C.T. Kraft, R.W. Murray, *J. Am. Chem. Soc.* 1998 (1906) 120.
- [73] C.S. Weisbecker, M.V. Merritt, G.M. Whitesides, *Langmuir* 12 (1996) 3763.
- [74] D.T. Robb, V. Privman, *Langmuir* 24 (1) (2008) 26.
- [75] D.A. Giljohann, D.S. Seferos, W.L. Daniel, M.D. Massich, P.C. Patel, C.A. Mirkin, *Angew. Chem. – Int. Ed.* 49 (2010) 3280.